



Enhancing solar energy conversion efficiency: Thermophysical property predicting of MXene/Graphene hybrid nanofluids via bayesian-optimized artificial neural networks

Dheyaa J. jasim^a, Husam Rajab^b, As'ad Alizadeh^c, Kamal Sharma^d, Mohsen Ahmed^e, Murizah Kassim^{f,g}, S. AbdulAmeer^{h,i}, Adil A. Alwan^j, Soheil Salahshour^{k,l,m}, Hamid Maleki^{n,*}

^a Department of Petroleum Engineering, Al-Amarah University College, Maysan, Iraq

^b College of Engineering, Mechanical Engineering Department, Alasala University, King Fahad Bin Abdulaziz Rd., P.O.Box: 12666, Amanah, 31483, Dammam, Kingdom of Saudi Arabia

^c Department of Civil Engineering, College of Engineering, Cihan University-Erbil, Erbil, Iraq

^d Institute of Engineering and Technology, GLA University, Mathura, U.P. 281406, India

^e Imam Abdulrahman Bin Faisal University, P.O. Box 1982, Dammam, 31441, Eastern Province, Kingdom of Saudi Arabia

^f Institute for Big Data Analytics and Artificial Intelligence (IBDAAI), Universiti Teknologi MARA, 40450, Shah Alam, Selangor, Malaysia

^g School of Electrical Engineering, College of Engineering, Universiti Teknologi MARA, 40450, Shah Alam, Selangor, Malaysia

^h Department of Automobile Engineering, College of Engineering, Al-Musayab, University of Babylon, Iraq

ⁱ Ahl Al Bayt University, Kerbala, Iraq

^j College of Technical Engineering, National University of Science and Technology, Dhi Qar, 64001, Iraq

^k Faculty of Engineering and Natural Sciences, Istanbul Okan University, Istanbul, Turkey

^l Faculty of Engineering and Natural Sciences, Bahcesehir University, Istanbul, Turkey

^m Department of Computer Science and Mathematics, Lebanese American University, Beirut, Lebanon

ⁿ Renewable Energy Research Group, Isfahan, Iran

ARTICLE INFO

Keywords:

Solar energy conversion
PVT solar panels
Artificial neural network
Machine learning
MXene
Graphene

ABSTRACT

Accurately predicting thermo-physical properties (TPPs) of MXene/graphene-based nanofluids is crucial for photovoltaic/thermal solar systems, driving focused research on developing precise TPP predictive models. This study presents optimized multi-layer perceptron neural network (MLPNN) models, leveraging Bayesian optimization to refine architectural and training hyperparameters, including hidden layers, neurons, activation functions, standardization, and regularization terms. A comparative analysis of Bayesian acquisition functions—the probability of improvement (POI), lower confidence bound (LCB), expected improvement (EI), expected improvement plus (EIP), expected improvement per second plus (EIPSP), and expected improvement per second (EIPS)—demonstrated that the POI-MLPNN achieves the most accurate results, as evidenced by the lowest MAPE of 1.0923 % and exceptional consistency with an R-value of 0.99811. The EI-MLPNN and EIP-MLPNN models recorded the same outputs. The EI/EIP-MLPNN (R = 0.99668) model excels in consistency over LCB-MLPNN (R = 0.99529) and EIPSP-MLPNN (R = 0.99667). The optimized models offer a reliable, cost-efficient alternate for experimental and computational TPP analyses. Leveraging insights from these models enables better control over nanofluid TPPs in solar systems, enhancing energy conversion efficiency.

1. Introduction

Nanofluids, precisely engineered colloidal suspensions of nano-materials (NMs) in a base fluid, have gained significant attention due to their potential to improve heat transfer and thermophysical properties (TPPs) in various applications [1,2]. Extensive research has established

that the heat transfer performance of nanofluids is strongly influenced by the composition of the mixture, including the choice and size of nanoparticles, as well as the base fluid used [3,4]. This highlights the importance of carefully considering and manipulating these factors in nanofluid design. Empirical evidence has demonstrated that the addition of NMs like MWCNT [5,6], Fe₃O₄ [7], TiO₂ [8], Al₂O₃ [9], CuO

* Corresponding author.

E-mail address: H_Maleki_2024@yahoo.com (H. Maleki).

<https://doi.org/10.1016/j.rineng.2024.102858>

Received 2 July 2024; Received in revised form 8 August 2024; Accepted 4 September 2024

Available online 7 September 2024

2590-1230/© 2024 The Authors. Published by Elsevier B.V. This is an open access article under the CC BY-NC-ND license (<http://creativecommons.org/licenses/by-nc-nd/4.0/>).

[10], MgO [11], ZnO [12], CeO₂ [13], and SiO₂ [14] to various based fluids effectively enhances the specific heat capacity (SHC), thermal conductivity (TC), and dynamic viscosity (DV) of the resulting nanofluids. In addition, the use of binary/ternary hybrid nanofluids, which combine different types of NMs, has shown great promise in enhancing the thermophysical properties compared to mono nanofluids [15,16]. This presents an advantage in terms of performance, further highlighting the potential of nanofluids in various applications such as heat exchangers, heat pipes, microchannel heat sinks, solar collectors, drilling fluids, filtration control, electrical cooling mechanisms, and biomedical engineering [17–22]. The significant importance attributed to nanoparticles has spurred extensive research efforts to identify materials with exceptional efficacy tailored explicitly for various applications. These efforts led to the introduction of two-dimensional materials with improved properties [23]. Graphene-based NMs can be referred to as among the most cutting-edge two-dimensional materials that have been introduced. These NMs have garnered considerable interest owing to their exceptional physicochemical and thermophysical properties [24]. Graphene-based NMs possess unique properties in structure, optics, thermals, electronics, and mechanics, making them well-suited for a wide range of biomedical applications [25–27]. The physical, optical, and electrochemical properties of these NMs have played a vital role in advancing susceptible and selective biosensor devices [28]. Additionally, Graphene's exceptional properties, including high surface area, conductivity, and ease of functionalization, make it an ideal platform for synthesizing metallic nanoparticles-graphene nanocomposites [29].

Graphene-based nanomaterials (GNMs), with their exceptional TPPs, are an ideal nanomaterial for nanofluid preparation [30]. GNMs have shown significant potential for enhancing heat transfer due to their high aspect ratio and thermal conductivity [31]. Studies on graphene nanofluids have revealed that higher GNM concentrations and fabrication temperatures improve thermal conductivity [32]. Recent research revealed that including graphene in nanofluids substantially impacts TC, resulting in enhancements ranging from 1.2 % to 83.4 % [33]. Copper nanoparticles coated with graphene NMs demonstrate significantly higher TC, ranging from 3.7 to 18.2 times that of copper nanofluids [34]. Graphene oxide nanofluids also exhibit increased TC at higher mass concentrations [35]. Equilibrium molecular dynamics simulations have confirmed that nanofluids' TC increases as the graphene nanosheet loading fraction rises [36]. The addition of GNMs to nanofluids has an impact on the fluid's dynamic viscosity. At low GNM concentrations, the base fluid's viscosity decreases, with a maximum reduction of 17 % observed at a concentration of 0.5×10^{-3} wt % and 50 °C [37]. However, at higher GNM concentrations, the viscosity of graphene nanofluids is similar to most nanofluids [38]. The presence of graphene nanoflakes reduces the time required to reach desired viscosities in hydrate systems [39]. Adding graphene nano-plates to non-aqueous nanofluids affects viscosity and provides lubrication effects depending on the GNM concentrations [40]. Factors like shear rate, concentration, base fluids, and temperature influence the rheological properties of graphene-based nanofluids.

On the other hand, in recent years, MXene NMs, notably Ti₃C₂T_x, have gained prominence due to their distinctive properties and wide-ranging applications. These materials exhibit high electrical and thermal conductivity, a large surface area, and hydrophilicity, making them well-suited for diverse purposes. Extensive studies on their properties have yielded promising outcomes across multiple disciplines [41,42]. MXene nanomaterials have found applications in various industries, including energy systems, optics, electromagnetic interference shielding, water purification, and photocatalysis, showcasing their versatility and potential impact [43,44]. Additionally, MXenes hold promise in biomedical fields such as tissue engineering, wound healing, antibacterial agents, and biosensors, thanks to their biocompatibility, biodegradability, and antibacterial properties [45]. Furthermore, MXene-based nanofluids have diverse applications, including in photovoltaic/thermal (PV/T) solar systems. In this regard, Wang et al. [46]

found that MXene/water nanofluid achieved a maximum photo-thermal conversion (PTC) efficiency of 63.35 %, surpassing graphene-based nanofluids. Aslfattahi et al. [47] demonstrated the high potential of MXene nanofluids in solar thermal applications when added to soybean oil. Said et al. [48] reported a significant increase in TC (70–89 %) in a parabolic trough collector using silicon oil/MXene nanofluid. These findings underline the positive impact of MXene nanofluids on PV/T solar systems.

Recent research has clarified the significant potential of MXene NMs in improving the TPPs of nanofluids. In a study by Mao et al. [49], notable enhancements in the TC of nanofluids were discovered. The water/EG/MXene and water/MXene nanofluids exhibited improvements of 27.3 % and 30.6 % in TC, respectively. Despite a slight increase in DV, the researchers foresee MXene-based nanofluids holding significant promise for cooling applications. Bao et al. [50] investigated the stability, TC, and DV of Ti₃C₂T_x MXene/EG nanofluid. They observed a noteworthy 9.64 % increase in TC of nanofluid. Moreover, the DV of the nanofluid, at a concentration of 1 vol%, was significantly lower than that of nanofluids containing MWCNT and graphene at a concentration of 0.1 vol%. The produced nanofluid exhibited excellent stability over 30 days, showcasing its promising performance.

Artificial intelligence (AI) is an interdisciplinary field within computer science that focuses on creating and developing intelligent machines capable of performing tasks traditionally requiring human intelligence [51]. These machines are designed to exhibit cognitive abilities such as learning, reasoning, problem-solving, and decision-making. AI encompasses subfields such as machine learning (ML), natural language processing, computer vision, and robotics [52]. In recent years, ML techniques have emerged as powerful modeling tools within AI, particularly for complex systems [53–55]. Nanofluids, with their intricate TPPs, present a challenging system to model accurately, especially when multiple input variables are involved [56]. By employing ML techniques, modeling nanofluids' TPPs offers the potential to reduce costs and save time that would otherwise be spent on frequent experimental investigations. Table 1 provides an overview of recent applications of machine learning in predicting the TPPs of nanofluids containing GNMs or MXenes.

The machine learning techniques presented in Table 1, including artificial neural networks (ANNs), Gaussian process regression (GPR) [74], boosted regression trees (BRT) [75], and support vector machines (SVM) [76], are widely recognized and acknowledged. Among them, ANNs have gained prominence due to their exceptional ability to establish effective relationships between dependent and independent variables. However, it is worth noting that other machine learning methods, such as multivariate adaptive regression spline (MARS) [77], kernel extreme learning machine (KELM) [77], random forest (RF) [78], least-squares support vector machine (LSSVM) [79], K-nearest neighbors (KNN) [79], radial basis function neural network (RBFNN) [79], locally weighted linear regression (LWLR) [80], multigene genetic programming (MGPP) [81], AdaBoost regression (ABR) [82], extra tree regression (ETR) [82], extended Kalman filter (EKF) [83], and adaptive neuro-fuzzy inference system (ANFIS) [84] also exhibit the significant potential of AI algorithms in real-world applications. These algorithms have demonstrated the capacity to reduce financial and computational costs while accurately predicting nanofluids' various TPPs.

The reviewed studies provide clear evidence of the significance of nanofluids' thermophysical properties in various systems. Particularly noteworthy is the importance of nanofluids containing MXenes [46–48] and graphene-based nanomaterials [32–35] due to their widespread applications, especially in renewable energy. This research focuses on accurately predicting dynamic viscosity, a crucial thermophysical property essential for designing energy systems. According to Table 1, neural network-based models show high precision in predicting the TPPs. Therefore, in this study, multilayer perceptron neural networks (MLPNN) are used to predict the dynamic viscosity of nanofluids containing MXene and graphene. To further improve the MLPNN-based DV

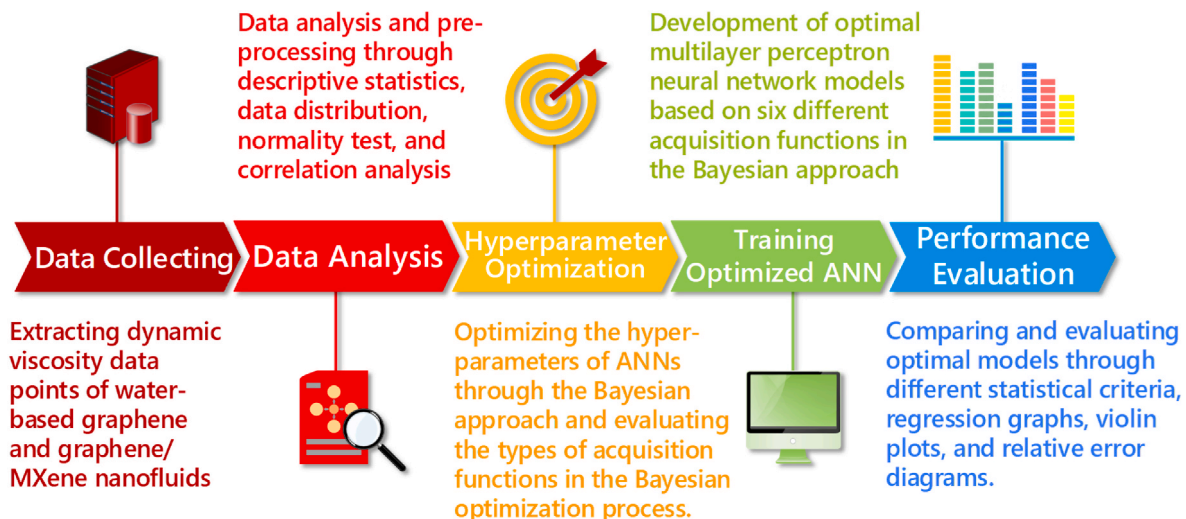
Table 1

A summary of recent studies presenting ML-based models to predict TPPs of nanofluids containing GNMs or MXenes.

Reference	Year	TPP	Base Fluid	Nanomaterials	ML Method	Accuracy
[57]	2020	TC	Water	GO-SiO ₂	ANN	R ² = 0.999
[58]	2021	TC	EG-Water	GO-CuO	ANN	R = 0.999103
[59]	2021	DV	EG	Graphene	ANN	R ² = 0.9978
[60]	2021	DV	Palm oil	MXene	ANN	R = 0.99975
[61]	2021	TC	EG-Water	GO-Al ₂ O ₃	ANN	R = 0.999
[62]	2021	DV	Aqueous solution of ionic liquid	MXene	ANN	R ² = 0.99986
[62]	2021	TC	Aqueous solution of ionic liquid	MXene	ANN	R ² = 0.9946
[63]	2021	DV	Palm oil	MXene	SVM	R ² = 0.99987
[64]	2022	DV	Diethylene glycol and ionic liquid	MXene	ANN	R = 0.99963
[64]	2022	SHC	Diethylene glycol and ionic liquid	MXene	ANN	R = 0.99872
[64]	2022	TC	Diethylene glycol and ionic liquid	MXene	ANN	R = 0.99783
[65]	2022	DV	EG	rGO-Fe ₃ O ₄ -TiO ₂	BRT, SVM, and ANN	R = 0.9960 to 0.9979
[66]	2022	DV	Water	Graphene	ANN	R ² = 0.999
[67]	2022	TC	Silicone oil	MXene	ANN	R = 0.99687
[65]	2022	Density	EG	rGO-Fe ₃ O ₄ -TiO ₂	BRT, SVM, and ANN	R = 0.9973 to 0.9989
[68]	2022	DV, TC, and SHC	Aqueous Ionic liquid solution	MXene	GPR	R = 0.9942 to 0.9998
[68]	2022	DV, TC, and SHC	Aqueous Ionic liquid solution	MXene	SVM	R = 0.9741 to 0.9958
[69]	2023	DV	Water	GO-MXene	ANN	R = 0.9926
[69]	2023	SHC	Water	GO-MXene	ANN	R = 0.9913
[69]	2023	TC	Water	GO-MXene	ANN	R = 0.9989
[70]	2023	DV	Water	MXene	ANN	MSE = 4.7333E-04
[70]	2023	TC	Water	MXene	ANN	MSE = 1.1160E-04
[71]	2023	TC and DV	EG-Water	Graphene-CuO-Al ₂ O ₃	ANN	R = 0.99496
[72]	2023	TC	Water	GO-CuO	BRT and SVM	R ² = 0.9923 to 0.9988
[72]	2023	DV	Water	GO-CuO	BRT and SVM	R ² = 0.9976 to 0.9992
[73]	2023	TC and DV	Water	GO-Al ₂ O ₃	SVM and ANN	R = 0.9715 to 0.9991

predictive models, Bayesian optimization is applied for the first time to fine-tune hyperparameters. Additionally, this study offers a novel comparison of various acquisition functions for optimizing MLPNN hyperparameters, including expected improvement per second plus (EIPSP), expected improvement (EI), expected improvement plus (EIP), expected improvement per second (EIPS), lower confidence bound (LCB), and probability of improvement (POI). This comparison is one of the key aspects of the present study that has been neglected in previous research. Its precise adjustment can reveal the potential of Bayesian optimization and serve as a basis for improving the modeling process in future studies. The models developed in this research provide engineers with profound insights into the dynamic viscosity of the nanofluid under investigation, enabling accurate predictions even in out-of-test conditions. These advancements have significant implications for enhancing efficiency and effectiveness across various industries, ranging from energy production systems to thermal management. Furthermore, the present research explicitly outlines its alignment with the sustainable development goals (SDGs), thereby highlighting its broader societal

implications and strengthening the emphasis on research with positive impact. By demonstrating the potential of the developed models to optimize energy consumption and advance sustainable nanofluid-based solar technologies, we establish a clear connection to SDGs 7 (Affordable and Clean Energy) and 9 (Industry, Innovation, and Infrastructure). This enhancement significantly strengthens the research's contribution to the global sustainability agenda. Moreover, the developed models considerably reduce the costs associated with experimental investigations and computational simulations, making them highly practical and cost-effective. Fig. 1 provides a comprehensive roadmap outlining the distinct phases of the present research. A dedicated section for thorough review and analysis accompanies each step. The first two steps involve the introduction of the database obtained from experimental research, followed by data analysis and pre-processing. Subsequently, the third stage focuses on incorporating machine learning algorithm and the optimization process for hyperparameters. This stage entails the integration of artificial neural networks with the Bayesian approach to optimize the hyperparameters effectively. Moving forward, the

**Fig. 1.** Roadmap of the present study.

subsequent step centers on developing predictive models, with a specific emphasis on evaluating various acquisition functions within the Bayesian framework. Finally, in the last stage, the developed models undergo evaluation using different statistical criteria, and comparisons are made utilizing various graphical tools.

2. Datasets

ANNs allow programs to recognize patterns and solve common problems in artificial intelligence, machine learning [85–88]. The construction of enhanced predictive ANN-based models was based on employing empirical data sets, as delineated in the study conducted by Jin et al. [89]. The researchers quantitatively assessed the dynamic viscosity characteristics of aqueous hybrid nanofluids infused with graphene nanomaterials and MXene nanocomposites. The nanomaterials' mass fraction (MF) was meticulously evaluated within a spectrum of 0–2%, and thermal conditions were methodically varied between 5 and 60 °C during the experimentation. During the synthesis of mono and hybrid nanofluids, varied proportions of graphene and MXene nanomaterials were considered. The preliminary stage in developing models predicated on machine learning entails an in-depth delineation of the determinants affecting dependent variables. It is evident that many parameters pertaining to the base fluid and the NMs exert partial to substantial influence on the dynamic viscosity of the nanofluid. Based on antecedent investigations [56,78,81], independent variables that harbored considerable potential to impact the dynamic viscosity of diverse nanofluids were subjected to a systematic sequence of heuristic evaluations. This process was undertaken with the objective of selecting the parameters with maximum efficacy in accordance with the present dataset. This methodology enhances the accuracy and expedience of computational procedures while concurrently endeavoring to attenuate the intricacy inherent in the models to a feasible extent. Ultimately, it was ascertained that the mass fraction, temperature, and the MXene ratio emerge as the paramount determinants.

Table 2 delineates the descriptive statistical information for the assorted variables under consideration. The analysis of skewness and kurtosis values offers a quantitative mechanism for appraising the extent of normal (Gaussian) distribution conformity exhibited by the variables. Referencing antecedent research [90–92], the discernment of a Gaussian distribution within the dataset is contingent upon the containment of skewness values within the range of -1 to $+1$ and the limitation of kurtosis values to the confines of -2 to $+2$. Considering both criteria concurrently, one can assert that the temperature and the mass fraction conform to a Gaussian distribution. Furthermore, as illustrated in the table, the MXene ratio and the DV exhibit the most pronounced kurtosis among the independent and dependent variables. This suggests a divergence from the Gaussian distribution and a significant discrepancy between their median and mean values.

The box plot depicted in Fig. 2 graphically represents the dispersion of normalized data across all variables. A box plot serves as a visual depiction of dataset distribution that illustrates a data's median, quartiles, and outliers. The central box spans the first quartile (Q1) to the third quartile (Q3), with a line at the median. Whiskers stretch from the

Table 2
Descriptive statistics of observations.

Descriptive statistics	Inputs			Target
	Temperature (°C)	MF (wt %)	MXene ratio (%)	DV (mPa·s)
Minimum	5	0	0	0.5818
Maximum	60	2	50	1.7532
Mean	30.7143	1.2333	9.4444	1.0968
Std. Deviation	19.1315	0.8106	16.5371	0.2804
Skewness	0.1247	-0.4097	1.6461	0.2564
Kurtosis	1.6690	1.4993	4.3127	2.2695

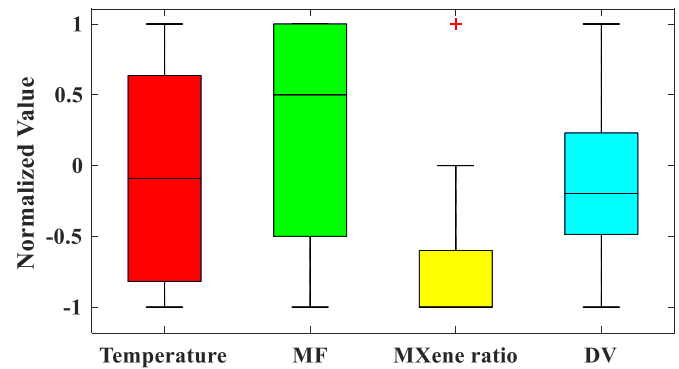


Fig. 2. Box plots of the studied variables.

box to the data's min and max that fall within 1.5 times the interquartile range (IQR), and points beyond this are outliers. In order to achieve a consolidated graphical representation of all variables, data normalization within the scope of $[-1, 1]$ is performed in the following form:

$$x_{norm} = \frac{x - x_{min}}{x_{max} - x_{min}} \times 2 - 1 \quad (1)$$

To facilitate an enhanced understanding of the data's dispersion, Fig. 3 elucidates the frequency distributions of both independent and dependent variables via histograms. It is particularly noteworthy that Fig. 3(a) accentuates the predominance of data points within a homogeneous temperature range from 5 to 60 °C. Moreover, an inspection of Fig. 3(b) discloses that a considerable segment of the dataset demonstrates mass fractions gravitating towards the extremities, proximate to the minimum (0 wt%) and the maximum (2 wt%) thresholds. In addition, Fig. 3(c) provides evidence that the existence of MXene is principally infrequent within the dataset, signifying a dominant occurrence of graphene-water mono-phase nanofluids. There exists a limited frequency of MXene/graphene-water hybrid nanofluids, evidenced by instances where the mass fraction of MXenes amounts to 25–50 % of the nanocomposite materials.

The relationship between dependent and independent variables is analyzed using the Kendall correlation coefficient (KCC) [93]. The KCC, or Kendall's tau coefficient, is a non-parametric statistic that measures the ordinal association between two measured quantities. It evaluates the strength and direction of the relationship, indicating whether pairs of observations are concordant (similar rankings in both variables) or discordant (dissimilar rankings). The KCC is calculated in the following two steps.

1. Definition of pairs:

- A pair of observations (x_i, y_i) and (x_j, y_j) is concordant if both elements agree in order: if $x_i > x_j$ and $y_i > y_j$ or $x_i < x_j$ and $y_i < y_j$.
- A pair of observations is discordant if the elements disagree in order: if $x_i > x_j$ and $y_i < y_j$ or $x_i < x_j$ and $y_i > y_j$.

2. Formula:

$$KCC = \frac{C - D}{0.5n(n - 1)} \quad (2)$$

where, C is the number of concordant pairs, D is the number of discordant pairs, and n is the number of observations. The KCC ranges from -1 to 1 , with a value of 1 implying perfect agreement, -1 indicating perfect disagreement, and 0 suggesting no association. Essentially, KCC assesses the rank correlation by comparing the number of concordant and discordant pairs relative to the total pairs, which is valuable in scenarios where the assumptions of parametric tests cannot be met.

Fig. 4 portrays the KCCs as a correlogram illustrating the interdependencies among different variables. According to the information in Fig. 4, the temperature exhibits the most substantial

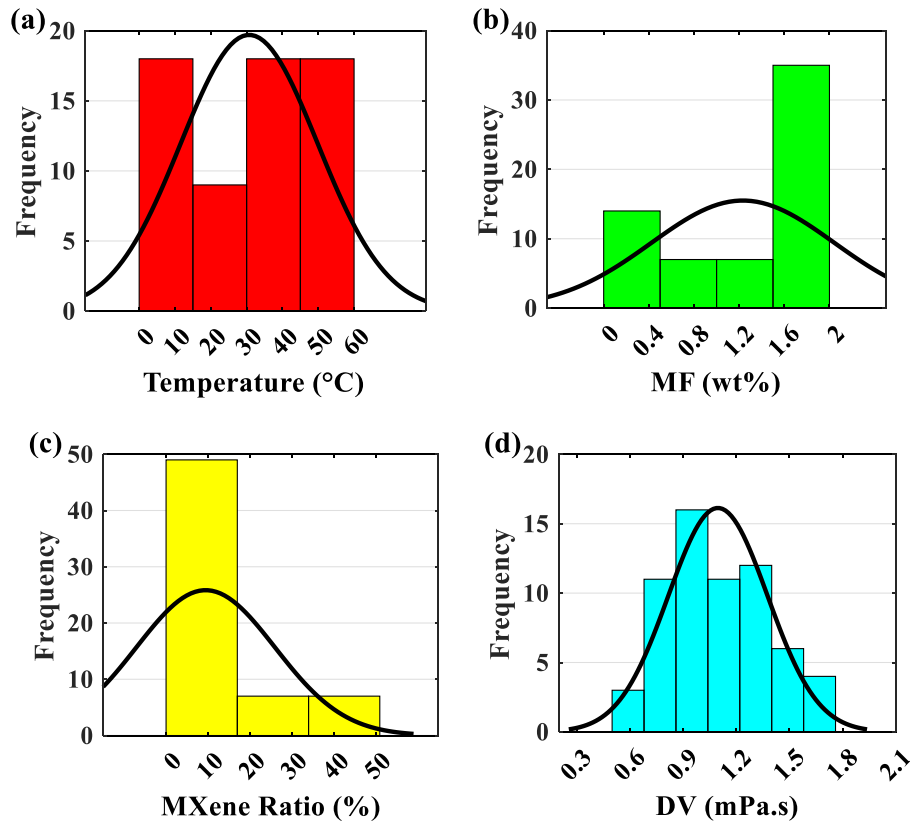


Fig. 3. Histogram of the studied variables.

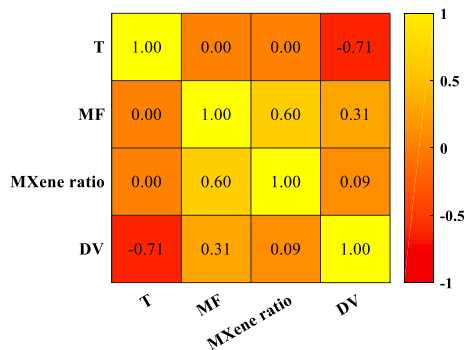


Fig. 4. Correlogram of KCC between various variables.

correspondence with the DV, evidenced by a KCC of -0.71 . The ensuing analysis delineates a middling degree of correlation, with a KCC of 0.31 , between the MF and the DV. At the same time, the most tenuous link, denoted by a KCC of 0.09 , is detected between the DV and the MXene proportion.

3. Methodology

3.1. Multilayer perceptron neural network (MLPNN)

A Multilayer Perceptron (MLP) is a class of feed-forward ANN that comprises multiple layers of nodes, each layer fully connected to the next one. An MLP is structured with a series of layers: the initial layer takes in the data, while the final layer delivers a verdict or inference based on that data [94,95]. Sandwiched between these, numerous intermediary layers, often referred to as hidden layers, serve as the core processing units of the network. ANN neurons function similarly to

neurons in a living organism, receiving inputs and generating corresponding outputs in response [96]. For instance, as shown in Fig. 5, a conventional architecture of an MLPNN is displayed, featuring a trio of input variables that feed into a singular output. This configuration incorporates a pair of hidden layers, the first housing three neurons and the second comprising two. MLPs employ a supervised learning process known as backpropagation to train their architectures. Within a given layer, every neuron forms a connection to each neuron in the subsequent layer. The connections are defined by specific weights that are dynamically refined throughout the training phase to optimize network performance. For regression problems, MLPs can model complex, nonlinear hypotheses that arise in real-world data, making them favorable for capturing intricate patterns that simpler linear regressions cannot.

The products of inputs and their corresponding weights are aggregated; this aggregate is then funneled through the node's activation

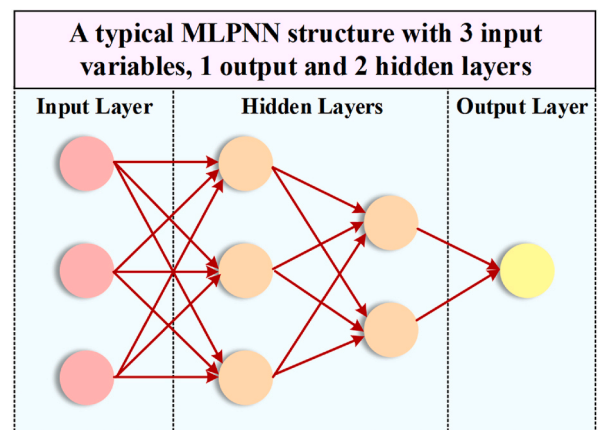


Fig. 5. A typical multilayer perceptron neural network structure.

function. This function is pivotal in deciding if, and to what degree, the signal should continue its journey through the network, ultimately influencing the outcome. Activation functions like the sigmoid, tanh, and ReLU introduce nonlinear properties to the network, which is essential for learning nonlinear representations in data. Training an MLP involves adjusting these weights through optimizing an error function, where the most popular method is gradient descent, in tandem with backpropagation, to compute the gradient efficiently. During this training phase, the model is iterated over many cycles (epochs) through the dataset, allowing it to learn progressively complex representations at each hidden layer, thereby improving its prediction accuracy with each pass.

Multiple elements influence the accuracy of the MLPNN-based regression model, with crucial factors including the number of hidden layers and their constituent neurons and the type of activation functions. Moreover, the present research incorporates the regularization term strength (λ) and a standardization term, which, although they receive less attention, play a significant role in fine-tuning the hyperparameters during the optimization of the MLPNNs.

Regularization represents a fundamental technique in machine learning, strategically implemented to restrain the complexity of models. Its primary purpose is to curb the occurrence of overfitting, ensuring that models generalize well to new, unseen data rather than capturing the noise in the training dataset. This technique involves augmenting the loss function with a penalty term, which reduces the model's complexity by controlling the magnitude of the parameters. In the current research, ridge regularization, a specific variant of regularization, is utilized. This approach incorporates a term, denoted by λ , into the loss function directly proportional to the sum of the squared values of the weights. The introduction of this term prompts the model to maintain smaller weights centered on zero, an adjustment that mitigates overfitting. Additionally, the study scrutinizes the effect of the standardization term, which can be set to either "true" or "false", on the precision of the model's outputs. This binary term determines whether each predictor variable should be centered and scaled based on its

or loss [98]. Through this historical information, the optimization process anticipates the utility of untested hyperparameters, thus prioritizing the exploration of more promising regions of the hyperparameter space. This method strategically directs the search using an acquisition function, which determines the potential value of new candidate points, balancing the need to explore uncertain areas against exploiting known high-performing zones. Consequently, Bayesian optimization is notably more efficient than grid or random searches, finding better solutions with fewer function evaluations [99].

The structure of the Bayesian optimization process relies heavily on its acquisition function, which directs the choosing of the next hyperparameters to assess [100]. Common types of acquisition functions include the probability of improvement (POI), lower confidence bound (LCB), and various types of expected improvement (EI) formulation [101].

4. Performance evaluation

To ascertain the performance of the assembled models predicated on MLPNN, a comprehensive suite of statistical criteria was utilized [102–104]:

$$\text{Mean squared error: } MSE = \frac{1}{n} \sum_{i=1}^n (Y_{i,Exp} - Y_{i,Pred})^2 \quad (2)$$

$$\text{Mean absolute percentage error: } MAPE(\%) = \frac{1}{n} \sum_{i=1}^n \left| \frac{Y_{i,Pred} - Y_{i,Exp}}{Y_{i,Exp}} \right| \times 100 \quad (3)$$

$$\text{Correlation coefficient: } R = \frac{\sum_{i=1}^n (Y_{i,Exp} - \overline{Y_{i,Exp}})(Y_{i,Pred} - \overline{Y_{i,Pred}})}{\sqrt{\sum_{i=1}^n (Y_{i,Exp} - \overline{Y_{i,Exp}})^2 \sum_{i=1}^n (Y_{i,Pred} - \overline{Y_{i,Pred}})^2}} \quad (4)$$

$$\text{Coefficient of determination: } R^2 = 1 - \frac{\sum_{i=1}^n (Y_{i,Pred} - Y_{i,Exp})^2}{\sum_{i=1}^n Y_{i,Exp}^2} \quad (5)$$

$$\text{Willmott's Index of Agreement: } I_A = 1 - \frac{\sum_{i=1}^n (Y_{i,Exp} - Y_{i,Pred})^2}{\sum_{i=1}^n (|Y_{i,Pred} - \overline{Y_{i,Exp}}| + |Y_{i,Exp} - \overline{Y_{i,Exp}}|)^2} \quad (6)$$

corresponding column's mean and standard deviation. By doing so, the study assesses how normalizing input variables influences the model's performance, potentially enhancing the predictive accuracy by treating all variables on a comparable scale and thereby improving the numerical stability of the optimization process.

3.2. Bayesian optimization

The Bayesian approach to hyperparameter optimization constitutes a sophisticated, probabilistic framework to identify the most effective hyperparameters for a machine learning model [97]. In contrast to exhaustive grid search or stochastic random search approaches, Bayesian optimization leverages accumulated knowledge from previous evaluations to make informed guesses about which hyperparameters are likely to yield improved performance in subsequent trials. By adopting a probabilistic model, often a Gaussian process, it assesses the relationship between hyperparameters and the target metric, such as model accuracy

$Y_{i,Exp}$, $Y_{i,Pred}$, and n denote the experimental data points, the corresponding predicted values, and the number of observations within the database. The metrics MSE and MAPE quantify the errors in the models, with values converging toward zero, indicative of enhanced precision within a given model. Additionally, the R , R^2 , and I_A function as quantitative indicators of the concordance between the model's predicted values and the empirical laboratory data, ranging within $[0, 1]$. A proclivity for these coefficients to approach unity indicates an augmented reliability of the model under scrutiny. In tandem with the previously delineated evaluative criteria for model assessment, the Relative Error (RE) offers a nuanced graphical depiction of the error corresponding to individual data points. The calculation of RE for each data point is achieved utilizing the following relationships:

$$RE_i(\%) = \frac{Y_{i,Exp} - Y_{i,Pred}}{Y_{i,Exp}} \times 100 \quad (7)$$

5. Models development

The architecture and training hyperparameters of MLPNNs substantially impact the models' outputs. These hyperparameters are amenable to a wide spectrum of potential values contingent upon the dataset's quality and quantity, in conjunction with the complexity inherent to the problem. As a result, the refinement of these hyperparameters is of paramount importance. In the present investigation, Bayesian optimization, considering six distinct acquisition functions, has been utilized to fine-tune the hyperparameters. This optimization technique aids in the optimal ascertainment of crucial parameters, containing the number of hidden layers, the number of neurons within them, the type of activation functions, the regularization term (Lambda), and the value of the standardized term.

In order to preserve model effectiveness while simultaneously preventing an excessive increase in model complexity, the hyperparameters under review are meticulously tuned within a rigorously defined range of permissible values. The number of hidden layers is constrained to a range from one to five. In an effort to manage the structural complexity of the models, the tally of neurons present within each hidden layer is restricted to a maximum of 20. Additionally, three activation functions are scrutinized: the sigmoid, hyperbolic tangent (tanh), and ReLU functions. The standardized term is dichotomous, furnishing the option to either implement input normalization (true) or abstain from it (false). Furthermore, the lambda hyperparameter is adjustable across a continuum that extends from 1E-07 to 1E+07. Electing values at the upper extremity of this range promotes simplification within the model, albeit at an increased likelihood of underfitting the dataset. Conversely, the selection of values at the lower extremity engenders a model with heightened complexity, which correspondingly bears an elevated risk of over-fitting.

The dataset germane to the current investigation is bisected into two segments: preponderance, constituting 80%, is earmarked for training, while the residual 20% is sequestered for the purpose of testing. Training data adjust neural network parameters; testing data, excluded from training, evaluate the network's post-training performance and ability to generalize to new data.

This research employs MATLAB (R2021b) coding to refine the hyperparameters of MLPNNs. Optimal hyperparameters are discerned utilizing a five-fold cross-validation technique, which entails segmenting the dataset into five distinct subsets and consecutively utilizing each as a validation set within the iterative training of a model on the residual four subsets. A demarcated search domain establishes the constraints for the hyperparameters, which undergo iterative refinement through Bayesian optimization, contingent upon the model's MSE performance metric ascertained on the validation subset. The methodology entails systematically training models with diverse permutations of hyperparameters, followed by their validation to chronicle performance scores. The set of hyperparameters that begets the most superior cumulative validation score is subsequently elected.

In the MATLAB coding framework, a constant random number generator instantiation (rng(default)) is deployed to ensure homogeneity during the initialization phase across the optimization approaches. Furthermore, invariant data points are systematically designated for the training and testing phases in constructing disparate MLPNN frameworks. The commitment to these methodological constants engenders conducive environment for a fair comparative examination between the optimized models and the acquisition functions associated with Bayesian optimization. Fig. 6 depicts the schematic representation of the prescribed process for designing Bayesian-based optimized MLPNN models.

6. Results

Implementing the proposed algorithm on different acquisition functions per 100 iterations results in an optimal specification for MLPNNs. Table 3 shows different statistical criteria for the superior model of each acquisition function in Bayesian optimization for testing and training data. As seen, Bayesian optimization using the POI acquisition function leads to more promising results on the testing data. According to the table POI-MLPNN model with MSE and MAPE, 1.93E-04 and 1.0923% record the lowest error on the testing data. Also, the outputs of this model on test data with $R = 0.99811$ and $R^2 = 0.99623$ show high consistency to experimental observations. Models EI-MLPNN and EIP-MLPNN go through the same optimization process during each iteration, leading to the same results. In general, EI/EIP-MLPNN, LCB-MLPNN, and EIPSP-MLPNN models have close performance. In terms of

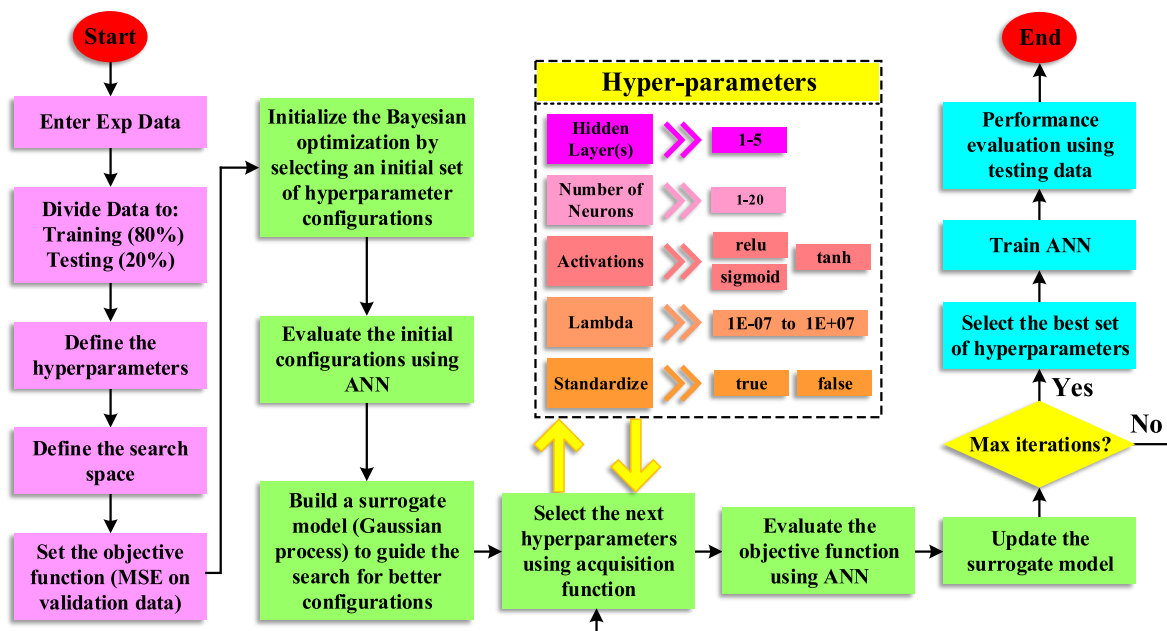


Fig. 6. Flowchart of present approach for developing fine-tuned MLPNN models.

Table 3

Accuracy of the best model developed by each acquisition function of the Bayesian approach.

Data	Acquisition Type	MSE	MAPE (%)	R	R ²	I _A
Testing Dataset	EIPSP	3.328E-04	1.4972	0.99667	0.99335	0.99811
	EI	3.350E-04	1.5124	0.99668	0.99338	0.99809
	EIP	3.350E-04	1.5124	0.99668	0.99338	0.99809
	EIPS	2.588E-03	4.3474	0.97263	0.94601	0.98512
	LCB	4.55E-04	1.4851	0.99529	0.99060	0.99750
Training Dataset	POI	1.93E-04	1.0923	0.99811	0.99623	0.99889
	EIPSP	4.708E-04	1.5283	0.99742	0.99484	0.99858
	EI	4.676E-04	1.5296	0.99743	0.99487	0.99859
	EIP	4.676E-04	1.5296	0.99743	0.99487	0.99859
	EIPS	3.094E-03	4.5868	0.98159	0.96352	0.99062
	LCB	2.88E-04	1.3694	0.99830	0.99661	0.99915
	POI	3.92E-04	1.5119	0.99770	0.99541	0.99884

Table 4

The optimized hyperparameters of the top three MLPNN models for each acquisition function of the Bayesian approach.

Acquisition Type	Rank	Number of Layers	Number of neurons	Activations	Standardize	Lambda
EIPSP	1	5	16-5-12-1-1	Tanh	True	1.2186E-05
	2	1	5	Relu	True	1.8548E-03
	3	4	5-1-7-18	Tanh	True	3.5727E-04
EI/EIP	1	4	16-1-6-18	Tanh	True	2.0043E-07
	2	2	3-2	Tanh	True	2.8754E-05
	3	5	4-9-16-5-20	Tanh	True	2.9017E-05
EIPS	1	5	9-15-19-5-6	Tanh	True	2.1774E-07
	2	4	15-3-12-3	Sigmoid	True	2.0310E-07
	3	3	9-18-3	Tanh	True	2.6614E-05
LCB	1	3	8-14-20	Tanh	True	5.8244E-06
	2	1	15	Tanh	True	2.0200E-07
	3	1	17	Relu	True	5.3412E-05
POI	1	2	6-6	Sigmoid	True	2.0077E-07
	2	1	9	Sigmoid	True	1.1723E-06
	3	5	15-1-3-2-19	Sigmoid	True	5.0338E-07

data consistency, EI/EIP-MLPNN model ($R = 0.99668$ and $R^2 = 0.99338$) is superior to LCB-MLPNN ($R = 0.99529$ and $R^2 = 0.99060$) and EIPSP-MLPNN ($R = 0.99667$ and $R^2 = 0.99335$), but in terms of errors generated by models, LCB-MLPNN model ($MAPE = 1.4851\%$) and EIPSP-MLPNN ($MSE = 3.328E-04$) are superior to EI/EIP-MLPNN ($MSE = 3.350E-04$ and $MAPE = 1.5124\%$). The EIPS-MLPNN Model has the weakest performance of the developed models, and $R = 0.97263$ and $MAPE = 4.3474\%$ result in the highest error and lowest consistency on the testing data.

Optimized hyperparameters for different acquisition functions are shown in Table 4. The results presented in Table 3 describe each model's best case (Rank 1). According to the table, a wide range of hidden layers from one to five numbers can lead to optimal conditions. Also, the number of neurons in each hidden layer can accept different values. In the best model, POI-MLPNN, the two hidden layers with six neurons embedded in each layer result in the best results in the testing stage. This shows that the most complex neural network architecture does not necessarily lead to optimal solutions but rather that optimal structural arrangement leads to appropriate outputs. According to the table, in most optimal states for EIPSP, EI/EIP, EIPS, and LCB acquisition functions, the Tanh function acts as an activator. However, in the top three models optimized by the POI acquisition function, the sigmoid function plays the activation role. The standardized parameter has "true" values in all cases of Table 4, which indicates the positive role of standardizing inputs in the output accuracy of models. Also, in most models, the lambda has a value smaller than $1E-04$, which shows the superiority of relatively complex models while not overfitting.

The graphical presentation provides valuable insight for a more detailed examination of the model's accuracy. For this purpose, Fig. 7 compares the regression graph of MLPNNs based on different acquisition functions. According to the figure, the testing data points in the POI-MLPNN model show greater conformity to the $Y = X$ line, indicating

the proximity of the model outputs and laboratory observations. These observations confirm the results seen in Table 3. Also, regarding the training data points, POI-MLPNN and LCB-MLPNN models provide a better performance that confirms the information presented in Table 3. The scattering of training and testing data points in the EIPS-based model and their high deviation from the $Y = X$ line indicate that this model is not performing well in the testing and training stages.

In order to focus on the deviation of the model outputs from the observations at the testing stage, the relative errors are depicted in Fig. 8. The margin of RE for different models is presented as follows.

- $-3.29\% < RE_{EIPSP} < 1.46\%$
- $-3.25\% < RE_{EI/EIP} < 1.60\%$
- $-6.21\% < RE_{EIPS} < 7.59\%$
- $-3.79\% < RE_{LCB} < 3.05\%$
- $-2.52\% < RE_{POI} < 2.66\%$

According to Fig. 8, the EIPS acquisition function in Bayesian-based optimization imposes a considerable relative error on the model outputs. The POI acquisition function results in an MLPNN model where the data points are generally closer to the zero-error line (ZEL). However, at some data points, especially with positive RE (above ZEL), EIPSP-MLPNN and EI/EIP-MLPNN models have less RE than the superior model (POI-MLPNN). In POI- and EIPS-based models, more points lie below ZEL, indicating that the models overestimate the observations. Conversely, in LCB-, EIPSP-, and EI/EIP-based models, most data points lie above the ZEL, meaning these models underestimate the experimental data.

In order to explore regions with better and more consistent predictions, comparing violin plots of actual data and predicted data can be helpful. Fig. 9 compares the violin plots derived from experimental data with the outputs of optimal MLPNN models. A violin plot is a sophisticated graphical tool that integrates the box plot with a kernel density

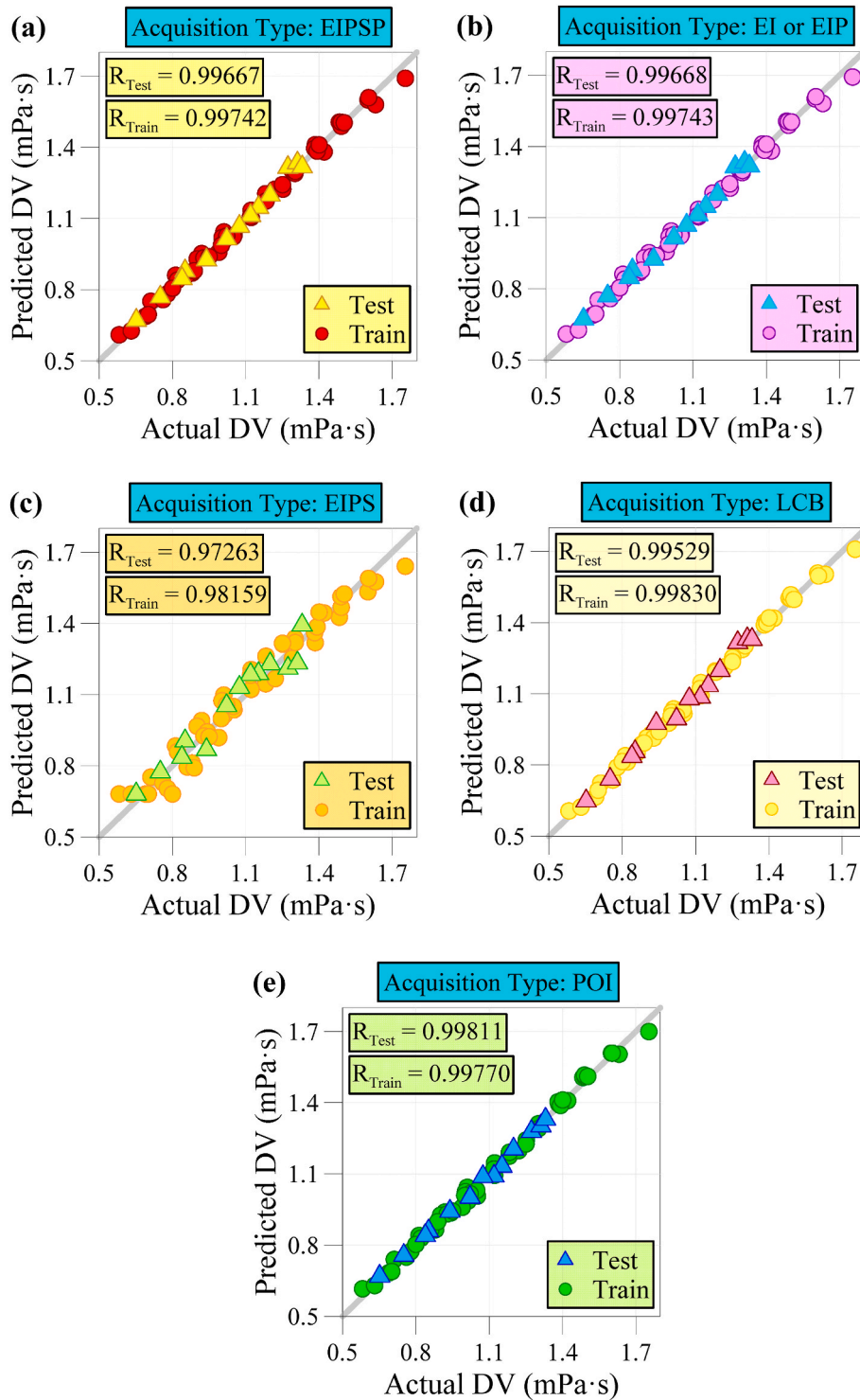


Fig. 7. Regression plots of MLPNN models optimized by Bayesian approach based on different acquisition functions.

plot to illustrate the distribution of data and its probability density function (PDF). This plot appears as a violin-shaped figure representing the data distribution's density, with the width of the plot at various levels signifying the frequency of data occurrence. Violin plots are particularly beneficial for analytic comparisons across multiple groups or data sets, as they convey the intricacies of data dispersion and central tendency metrics, providing a comprehensive visual summary of the data set's variability and central value comparisons. Fig. 9 shows that the output distribution from the POI-MLPNN model is more similar to the PDF of actual data. However, clear differences are visible in some

areas, such as $1 < DV < 1.2$ mPa s. In this particular area, the distribution of EI/EIP and EIPSP-based models is closer to the distribution of empirical data.

Furthermore, comparing the results of the superior developed model (POI-MLPNN) with experimental data and the findings of previous researchers can be advantageous. Jin et al. [89] proposed a discrete model containing ten formulas for the present data through curve fitting, considering different mass fractions of MXene and graphene nanomaterials. These relationships exhibited high accuracy in predicting the dynamic viscosity of nanofluids, with R^2 exceeding 0.99. Table 5

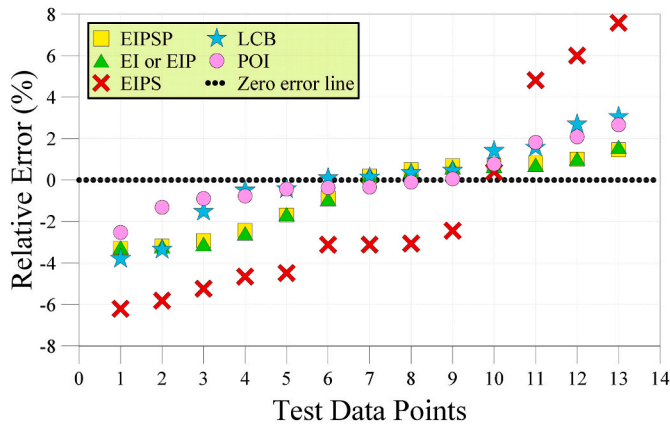


Fig. 8. The relative error of outputs in the testing phase for various optimal models.

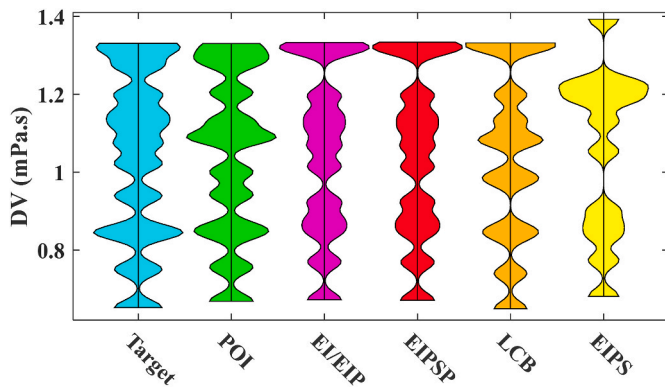


Fig. 9. Comparing violin graphs of optimized MLPNN models in the testing phase.

Table 5
Viscosity predictive formulas developed by Jin et al. [89].

Nanofluid		Viscosity formula
MF (wt%)	MXene ratio (%)	
0	0	$1.054 \times e^{-T/37.577} + 0.362$
0.1	0	$1.033 \times e^{-T/36.023} + 0.426$
0.5	0	$1.033 \times e^{-T/36.023} + 0.496$
1	0	$1.047 \times e^{-T/34.849} + 0.585$
1.5	0	$1.062 \times e^{-T/33.767} + 0.693$
2	0	$1.112 \times e^{-T/33.338} + 0.800$
2	10	$0.999 \times e^{-T/38.265} + 0.728$
2	25	$0.934 \times e^{-T/42.392} + 0.661$
2	50	$0.901 \times e^{-T/40.549} + 0.595$

presents the viscosity mathematical formulas. A comparison between the POI-MLPNN model and the results of Jin et al. [89] using experimental data reveals the accuracy of both models. While the model by Jin et al. [89] is discrete and not integrated, it serves as a valuable benchmark. Fig. 10 illustrates this comparison, demonstrating the high accuracy of the current model in predicting the dynamic viscosity of MXene/graphene-water hybrid nanofluid.

Fig. 11 illustrates the influence of input variables on the dynamic viscosity of nanofluid, as predicted via the superior model (POI-MLPNN). In accordance with theoretical anticipations, there is an inverse relationship between temperature elevation and the DV of nanofluids; an increase in temperature invariably leads to a decrease in DV. This phenomenon can be attributed to the augmented kinetic energy at

elevated temperatures, which diminishes the resistance to fluid flow. As thermal energy escalates, the nanoparticles exhibit more vigorous Brownian motion, thereby reducing the cohesive intermolecular forces within the base fluid and consequently lowering its viscosity. Furthermore, elevated thermal conditions mitigate the attractive forces between the particles, deterring aggregation that would otherwise reinforce viscosity. The thermal expansion of the base fluid under heat also contributes to a decrease in its density and an attendant decrease in DV.

Also, Fig. 11 confirms that an augmentation in the mass fraction of nanomaterials within a nanofluid is invariably associated with an increment in dynamic viscosity. Enhanced particle-particle interactions arise as a direct consequence of increased nanomaterial concentration. Such inter-particulate collisions contribute to a greater resistance to shearing forces within the fluid matrix, culminating in a heightened energy dissipation during flow. This necessitates an elevated input force to sustain the fluid movement, rendering the nanofluid more viscous. The aggregation of nanoparticles, prevalent at elevated concentrations, further compounds this rise in viscosity. This trend is consistent with established theoretical frameworks about the behavior of colloidal systems.

Moreover, Fig. 11 elucidates that an escalated proportion of MXenes within an MXene/graphene-water hybrid nanofluid correlates with a diminished DV. The distinct structural and chemical-physical characteristics of MXenes can explain the decrement in DV attributed to an increased MXene-to-graphene ratio. MXenes typically possess a more extended aspect ratio and exhibit flatter morphologies than graphene, potentially enabling more homogenous dispersion and diminishing rheological resistance - a contrast to the agglomeration tendency of graphene. The surface of MXenes, characterized by their hydrophilicity, favors enhanced compatibility with polar solvents, promoting colloidal stability and leading to a less viscous nanofluid, notwithstanding the augmented nanomaterial content. This is because MXenes facilitate the prevention of nanoparticle clustering that would otherwise result in increased viscosity.

7. Conclusion

The pivotal role of dynamic viscosity as a fundamental thermo-physical property in nanofluids composed of MXene and graphene-based nano-sized materials, particularly for use in photovoltaic/thermal solar systems, has spurred the scientific community to focus on creating precise and reliable predictive models. This study deployed models based on ANN to forecast dynamic viscosity precisely. The efficacy of MLP-type ANN models was enhanced by integrating Bayesian optimization. This technique was instrumental in fine-tuning the architectural and training hyperparameters of the ANN, which encompass the number of hidden layers, neurons within those layers, types of activation functions, standardized parameters, and regularization terms.

The optimization of MLPNN models has resulted in efficient and cost-effective alternatives to traditional methods, markedly decreasing the expenses linked to both experimental analyses and extensive computational simulations. The key findings from this research are summarized as follows.

- Optimized hyperparameters varied widely across different acquisition functions, demonstrating the flexibility and adaptability of the Bayesian optimization process in finding optimal configurations.
- Developed models showed strong performance metrics, with R and R² values above 0.99 for most acquisition functions, indicating high model accuracy and reliability.
- The POI acquisition function in Bayesian optimization yielded the best results in the testing phase. The POI-MLPNN model registered the slightest error with a MAPE of 1.0923 %. Outputs reflected high consistency with an R-value of 0.99811.

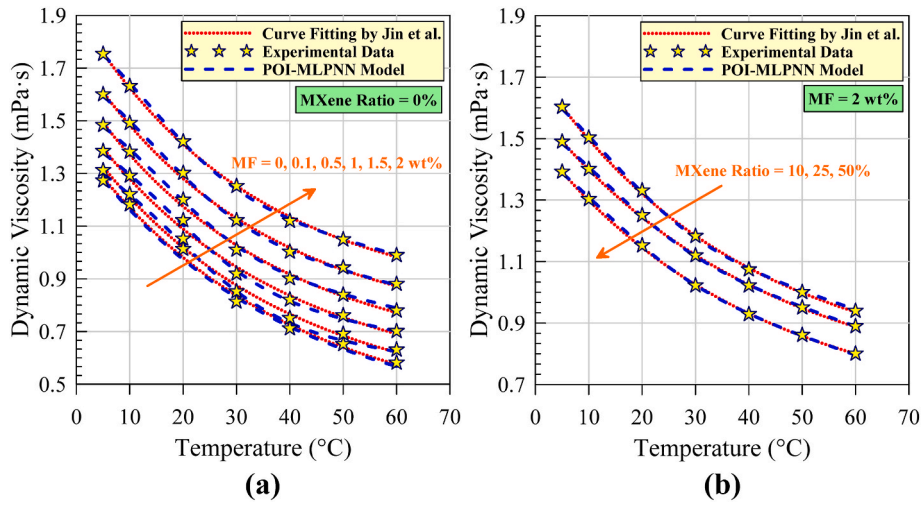


Fig. 10. Comparing the outputs of the POI-MLPNN model with the curve fitting results presented by Jin et al. [89] and the corresponding experimental data.

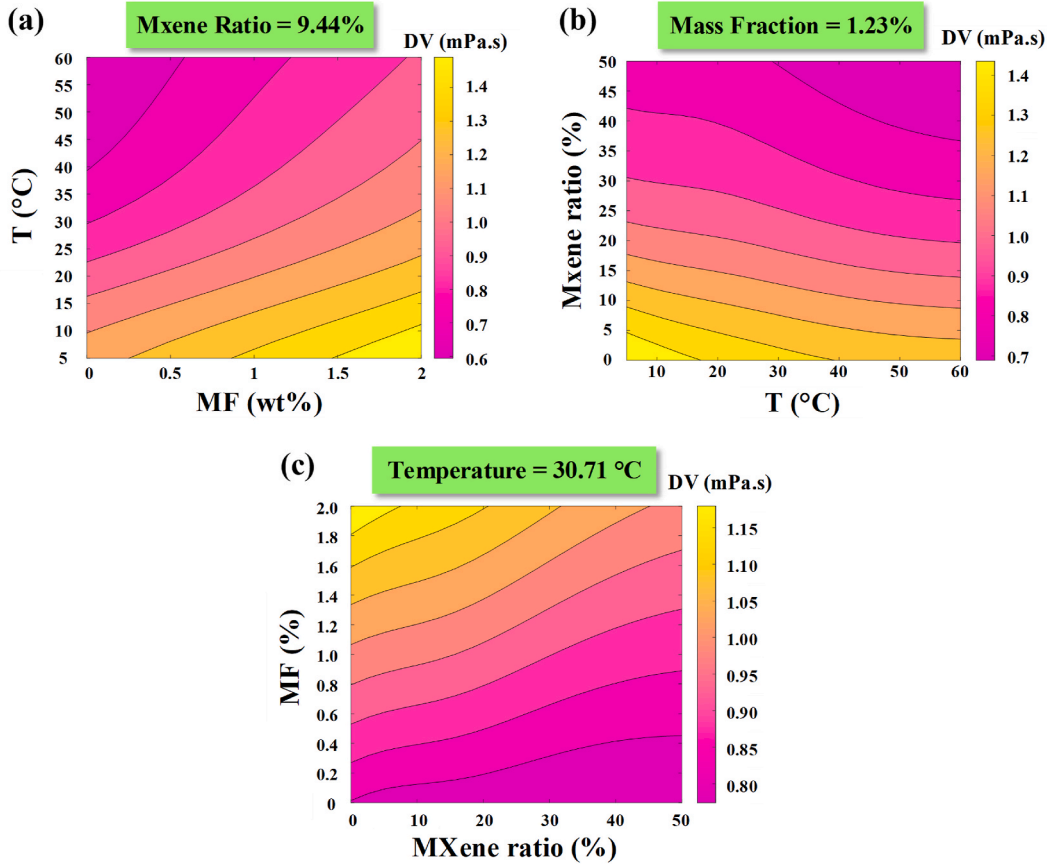


Fig. 11. Influence of inputs on the DV predicted by the best model (POI-MLPNN).

- The EI-MLPNN and EIP-MLPNN models showed similar performance due to identical optimization processes, achieving $R = 0.99668$ and $R^2 = 0.99338$.
- EI/EIP-MLPNN, LCB-MLPNN, and EIPSP-MLPNN models had close performance. In terms of consistency, EI/EIP-MLPNN model ($R = 0.99668$) is superior to LCB-MLPNN ($R = 0.99529$) and EIPSP-MLPNN ($R = 0.99667$).
- In terms of the error metrics, the LCB-MLPNN model, with a MAPE of 1.4851 %, and the EIPSP-MLPNN model, with an MSE of 3.328E-04,

- outperformed the EI/EIP-MLPNN models, which had a slightly higher MSE of 3.350E-04 and a MAPE of 1.5124 %.
- The RE analysis showed that the POI-MLPNN model maintained RE within a narrower range ($-2.52\% - 2.66\%$), confirming its robustness compared to other models.
- The optimal POI-MLPNN model used two hidden layers with six neurons each, indicating that a more complex neural network architecture is not necessarily superior but rather an optimal structural arrangement is key.

- The Tanh activator was prevalent in optimal states for EIPSP, EI/EPI, EIPS, and LCB acquisition functions. Conversely, the top three POI-optimized models predominantly utilized the sigmoid activation function.
- The consistent "true" value for the standardization parameter across all models highlights the critical role of input standardization in enhancing model performance.
- The study found that lambda values smaller than 1E-04 indicate that relatively complex models could be effective without overfitting, balancing complexity and generalization.

While the study effectively demonstrates the efficacy of MLPNN models enhanced by Bayesian optimization for predicting nanofluid viscosity, it has limitations. This research focuses on MXene and graphene-based nanofluids, which restricts generalizability, and the dataset may not cover all experimental conditions and inputs involved in real-world applications. This is due to the limited availability of experimental datasets. To address these limitations, future research should extend laboratory studies beyond the current data and conditions to generate sufficient data for the development of machine learning-based models. Additionally, integrating advanced machine learning techniques, such as deep learning with Bayesian optimization, can improve predictive accuracy.

Nomenclature

DV	Dynamic viscosity	(mPa-s)
I _A	Willmott's index of agreement	(-)
MF	Nanomaterials mass fraction	(wt%)
MXene ratio	Ratio of MXene weight to total nanomaterials weight	(-)
R	Correlation coefficient	(-)
R ²	Coefficient of determination	(-)
T	Temperature	(°C)
x	Variable	(-)
Subscripts		
max	Maximum	
min	Minimum	
norm	Normal	
Abbreviations		
ABR	AdaBoost regression	
AI	Artificial intelligence	
ANFIS	Adaptive neuro-fuzzy inference system	
ANN	Artificial Neural Network	
BRT	Boosted regression trees	
EG	Ethylene glycol	
EI	Expected improvement	
EIP	Expected improvement plus	
EIPS	Expected improvement per second	
EIPSP	Expected improvement per second plus	
EKF	Extended Kalman filter	
ETR	Extra tree regression	
GNM	Graphene-based nanomaterial	
GPR	Gaussian process regression	
IQR	Interquartile range	
KELM	Kernel extreme learning machine	
KNN	K-nearest neighbors	
KCC	Kendall correlation coefficient	
LCB	Lower confidence bound	
LSSVM	Least-squares support vector machine	
LWLR	Locally weighted linear regression	
MAPE	Mean absolute percentage error	
MARS	Multivariate adaptive regression spline	
MGGP	Multigene genetic programming	
ML	Machine learning	
MLPNN	Multi-layer perceptron neural network	
MSE	Mean squared error	
MWCNT	Multi-walled carbon nanotube	
NM	Nanomaterial	
PDF	Probability density function	
POI	Probability of improvement	
PTC	Photo-thermal conversion	
PVT	Photovoltaic/thermal	
RBFNN	Radial basis function neural network	

(continued on next column)

(continued)

RE	Relative error
RF	Random forest
RNG	Random number generator
SVM	Support vector machines
TC	Thermal conductivity
TPP	Thermophysical property

CRedit authorship contribution statement

Dheyaa J. jasim: Data curation, Formal analysis. **Husam Rajab:** Supervision, Investigation, Writing – original draft. **As'ad Alizadeh:** Formal analysis, Writing – original draft. **Kamal Sharma:** Formal analysis, Writing – original draft. **Mohsen Ahmed:** Investigation, Writing – original draft. **Murizah Kassim:** Supervision, Writing – review & editing. **S. AbdulAmeer:** Conceptualization, Data curation, Formal analysis. **Adil A. Alwan:** Supervision, Writing – review & editing. **Soheil Salahshour:** Supervision, Writing – review & editing, Conceptualization. **Hamid Maleki:** Investigation, Writing – original draft

Declaration of competing interest

The authors declare that they have no known competing financial interests or personal relationships that could have appeared to influence the work reported in this paper.

Data availability

No data was used for the research described in the article.

References

- [1] H. Maleki, M.R. Safaei, A.A. Alrashed, A. Kasaeian, Flow and heat transfer in non-Newtonian nanofluids over porous surfaces, *Journal of Thermal Analysis and Calorimetry* 135 (3) (2019) 1655–1666, <https://doi.org/10.1007/s10973-018-7277-9>.
- [2] H. Maleki, J. Alsarraf, A. Moganizadeh, H. Hajabdollahi, M.R. Safaei, Heat transfer and nanofluid flow over a porous plate with radiation and slip boundary conditions, *J. Cent. S. Univ.* 26 (5) (2019) 1099–1115, <https://doi.org/10.1007/s11771-019-4074-y>.
- [3] S.K. Das, S.U. Choi, W. Yu, T. Pradeep, *Nanofluids: Science and Technology*, John Wiley & Sons, 2007.
- [4] I. Zahmatkesh, et al., Effect of nanoparticle shape on the performance of thermal systems utilizing nanofluids: a critical review, *J. Mol. Liq.* 321 (2021) 114430, <https://doi.org/10.1016/j.molliq.2020.114430>.
- [5] M. Sepehrnia, H. Maleki, M.F. Behbahani, Tribological and rheological properties of novel MoO₃-GO-MWCNTs/5W30 ternary hybrid nanolubricant: experimental measurement, development of practical correlation, and artificial intelligence modeling, *Powder Technol.* 421 (2023) 118389, <https://doi.org/10.1016/j.powtec.2023.118389>.
- [6] S. Abbas, M. Nazar, S.F.F. Gillani, M. Naveed, M. Ahmad, Z.U. Nisa, A CPC fractional model of the heat and mass transport mechanism in Carbon nanotubes with slip effects on velocity, *Mod. Phys. Lett. B* 38 (13) (2024) 2450100, <https://doi.org/10.1142/s0217984924501008>.
- [7] A. Shahsavari, M. Sepehrnia, H. Maleki, R. Darabi, Thermal conductivity of hydraulic oil-GO/Fe₃O₄/TiO₂ ternary hybrid nanofluid: experimental study, RSM analysis, and development of optimized GPR model, *J. Mol. Liq.* (2023) 122338, <https://doi.org/10.1016/j.molliq.2023.122338>.
- [8] M. Sepehrnia, A. Shahsavari, H. Maleki, A. Moradi, Experimental study on the dynamic viscosity of hydraulic oil HLP 68-Fe₃O₄-TiO₂-GO ternary hybrid nanofluid and modeling utilizing machine learning technique, *J. Taiwan Inst. Chem. Eng.* (2023) 104841, <https://doi.org/10.1016/j.jtice.2023.104841>.
- [9] E. Elshazly, A.A. Abdel-Rehim, I. El-Mahallawi, 4E study of experimental thermal performance enhancement of flat plate solar collectors using MWCNT, Al₂O₃, and hybrid MWCNT/Al₂O₃ nanofluids, *Results in Engineering* 16 (2022) 100723, <https://doi.org/10.1016/j.rineng.2022.100723>.
- [10] I. Fazeli, M.R.S. Emami, A. Rashidi, Investigation and optimization of the behavior of heat transfer and flow of MWCNT-CuO hybrid nanofluid in a brazed plate heat exchanger using response surface methodology, *Int. Commun. Heat Mass Tran.* 122 (2021) 105175, <https://doi.org/10.1016/j.icheatmasstransfer.2021.105175>.
- [11] S. Mousavi, F. Esmailzadeh, X. Wang, A detailed investigation on the thermo-physical and rheological behavior of MgO/TiO₂ aqueous dual hybrid nanofluid, *J. Mol. Liq.* 282 (2019) 323–339, <https://doi.org/10.1016/j.molliq.2019.02.100>.

- [12] M.H. Esfe, S. Esfandeh, S. Saedodin, H. Rostamian, Experimental evaluation, sensitivity analysis and ANN modeling of thermal conductivity of ZnO-MWCNT/EG-water hybrid nanofluid for engineering applications, *Appl. Therm. Eng.* 125 (2017) 673–685, <https://doi.org/10.1016/j.applthermaleng.2017.06.077>.
- [13] M. Sepehrnia, H. Maleki, M. Karimi, E. Nabati, Examining rheological behavior of CeO₂-GO-SA/10W40 ternary hybrid nanofluid based on experiments and COMBI/ANN/RSM modeling, *Sci. Rep.* 12 (1) (2022) 1–22, <https://doi.org/10.1038/s41598-022-26253-4>.
- [14] A. Kumar, P. Chand, M. Hassan, Louvered finned car radiator with MWCNT-SiO₂ hybrid nanofluid: an experimental approach, *Powder Technol.* 415 (2023) 118176, <https://doi.org/10.1016/j.powtec.2022.118176>.
- [15] C. Pownraj, A. Valan Arasu, Effect of dispersing single and hybrid nanoparticles on tribological, thermo-physical, and stability characteristics of lubricants: a review, *Journal of Thermal Analysis and Calorimetry* 143 (2) (2021) 1773–1809, <https://doi.org/10.1007/s10973-020-09837-y>.
- [16] T. Zhang, et al., Optimization of thermophysical properties of nanofluids using a hybrid procedure based on machine learning, multi-objective optimization, and multi-criteria decision-making, *Chem. Eng. J.* (2024) 150059, <https://doi.org/10.1016/j.cej.2024.150059>.
- [17] K.V. Wong, O. De Leon, Applications of nanofluids: current and future, *Adv. Mech. Eng.* 2 (2010) 519659, <https://doi.org/10.1201/9781315163574-6>.
- [18] K.M. Jadeja, R. Bumataria, N. Chavda, Nanofluid as a coolant in internal combustion engine—a review, *Int. J. Ambient Energy* (2022) 1–18, <https://doi.org/10.1080/01430750.2022.2127891>.
- [19] S.K. Gupta, H. Verma, N. Yadav, A review on recent development of nanofluid utilization in shell & tube heat exchanger for saving of energy, *Mater. Today: Proc.* 54 (2022) 579–589, <https://doi.org/10.1016/j.matpr.2021.09.455>.
- [20] S. Abbas, et al., Soret effect on MHD Casson fluid over an accelerated plate with the help of constant proportional Caputo fractional derivative, *ACS Omega* 9 (9) (2024) 10220–10232, <https://doi.org/10.1021/acsomega.3c07311>.
- [21] S. Abbas, M. Ahmad, M. Nazar, M. Amjad, H. Ali, A.Z. Jan, Heat and mass transfer through a vertical channel for the Brinkman fluid using Prabhakar fractional derivative, *Appl. Therm. Eng.* 232 (2023) 121065, <https://doi.org/10.1016/j.applthermaleng.2023.121065>.
- [22] S. Abbas and M. Nazar, "Fractional analysis of unsteady magnetohydrodynamics Jeffrey flow over an infinite vertical plate in the presence of Hall current," *Math. Methods Appl. Sci.* doi: <https://doi.org/10.1002/mma.10326>.
- [23] W.-L. Li, et al., High-performance thin-film composite (TFC) membranes with 2D nanomaterial interlayers: an overview, *Results in Engineering* (2024) 101932, <https://doi.org/10.1016/j.rineng.2024.101932>.
- [24] Y.C. Shin, et al., Multifaceted biomedical applications of functional graphene nanomaterials to coated substrates, patterned arrays and hybrid scaffolds, *Nanomaterials* 7 (11) (2017) 369, <https://doi.org/10.3390/nano7110369>.
- [25] F. Perreault, A.F. De Faria, M. Elimelech, *Environmental applications of graphene-based nanomaterials*, *Chem. Soc. Rev.* 44 (16) (2015) 5861–5896.
- [26] S. Abbas, M. Nazar, Z.U. Nisa, M. Amjad, S.M.E. Din, A.M. Alanzi, Heat and mass transfer analysis of MHD Jeffrey fluid over a vertical plate with CPC fractional derivative, *Symmetry* 14 (12) (2022) 2491, <https://doi.org/10.3390/sym14122491>.
- [27] S. Abbas, Z.U. Nisa, M. Nazar, M. Amjad, H. Ali, A.Z. Jan, Application of heat and mass transfer to convective flow of Casson fluids in a microchannel with Caputo–Fabrizio derivative approach, *Arabian J. Sci. Eng.* 49 (1) (2024) 1275–1286, <https://doi.org/10.1007/s13369-023-08351-1>.
- [28] N. Ali, Graphene-based nanofluids: production parameter effects on thermophysical properties and dispersion stability, *Nanomaterials* 12 (3) (2022) 357, <https://doi.org/10.3390/nano12030357>.
- [29] A.O. Borode, N.A. Ahmed, P.A. Olubambi, M. Sharifpur, J.P. Meyer, Investigation of the thermal conductivity, viscosity, and thermal performance of graphene nanoplatelet-alumina hybrid nanofluid in a differentially heated cavity, *Front. Energy Res.* 9 (2021) 737915, <https://doi.org/10.3389/fenrg.2021.737915>.
- [30] W. Hu, et al., Graphene-based antibacterial paper, *ACS Nano* 4 (7) (2010) 4317–4323, <https://doi.org/10.1021/nn101097v>.
- [31] L. Ou, et al., Toxicity of graphene-family nanoparticles: a general review of the origins and mechanisms, *Part. Fibre Toxicol.* 13 (1) (2016) 1–24, <https://doi.org/10.1186/s12989-016-0168-y>.
- [32] P. Suvarnapaet, S. Pechprasarn, Graphene-based materials for biosensors: a review, *Sensors* 17 (10) (2017) 2161, <https://doi.org/10.3390/s17102161>.
- [33] H. Lin, et al., Recent advances in thermal conductivity and thermal applications of graphene and its derivatives nanofluids, *Appl. Therm. Eng.* 218 (2023) 119176, <https://doi.org/10.1016/j.applthermaleng.2022.119176>.
- [34] G.J. Olguin-Orellana, G.J. Soldano, J. Alzate-Morales, M.B. Camarada, M. M. Mariscal, Can graphene improve the thermal conductivity of copper nanofluids? *Phys. Chem. Chem. Phys.* 25 (7) (2023) 5489–5500, <https://doi.org/10.1039/d3cp00064h>.
- [35] X. Mei, X. Sha, D. Jing, L. Ma, Thermal conductivity and rheology of graphene oxide nanofluids and a modified predication model, *Appl. Sci.* 12 (7) (2022) 3567, <https://doi.org/10.3390/app12073567>.
- [36] S.P. Shit, N.K. Ghosh, S. Pal, Effects of graphene nanosheet on the enhancement of thermal conductivity of ethylene glycol nanofluids, *AIP Conf. Proc.* 2369 (1) (2021). AIP Publishing.
- [37] Y. Pakharukov, et al., The mechanism of oil viscosity reduction with the addition of graphene nanoparticles, *J. Mol. Liq.* 361 (2022) 119551, <https://doi.org/10.1016/j.molliq.2022.119551>.
- [38] A. McElligott, A. Guerra, C.Y. Du, A.D. Rey, J.-L. Meunier, P. Servio, Non-einsteinian viscosity behavior in plasma-functionalized graphene nanofluid systems, *ACS Appl. Energy Mater.* 5 (10) (2022) 12977–12990, <https://doi.org/10.1021/acsaem.2c02571>.
- [39] A. McElligott, A. Guerra, C.Y. Du, A.D. Rey, J.-L. Meunier, P. Servio, Dynamic viscosity of methane hydrate systems from non-Einsteinian, plasma-functionalized carbon nanotube nanofluids, *Nanoscale* 14 (28) (2022) 10211–10225, <https://doi.org/10.1039/d2nr02712g>.
- [40] S. Hamze, D. Cabaleiro, P. Estellé, Graphene-based nanofluids: a comprehensive review about rheological behavior and dynamic viscosity, *J. Mol. Liq.* 325 (2021) 115207, <https://doi.org/10.1016/j.molliq.2020.115207>.
- [41] Y. Pei, et al., Ti₃C₂T_x MXene for sensing applications: recent progress, design principles, and future perspectives, *ACS Nano* 15 (3) (2021) 3996–4017, <https://doi.org/10.1021/acsnano.1c00248>.
- [42] S.i. Massoumlari, S. Velioglu, Can MXene be the effective nanomaterial family for the membrane and adsorption technologies to reach a sustainable green world? *ACS Omega* 8 (33) (2023) 29859–29909, <https://doi.org/10.1021/acsomega.3c01182>.
- [43] B. Yao, J. Yao, Z. Fan, J. Zhao, K. Zhang, W. Huang, Rapid advances of versatile MXenes for electrochemical enzyme-based biosensors, immunosensors, and nucleic acid-based biosensors, *Chemelectrochem* 9 (11) (2022) e202200103, <https://doi.org/10.1002/celec.202200103>.
- [44] M. Rostami, P. Rezvaninia, A. Amiri, G.M. Ziarani, M.R. Ganjali, A. Badiie, Hybrid nano-architectural engineering of Ti₃C₂T_x MXene heterostructures for supercapacitor applications: a reviews, *Results in Engineering* (2024) 102227, <https://doi.org/10.1016/j.rineng.2024.102227>.
- [45] S. Li, et al., MXene-enhanced chitin composite sponges with antibacterial and hemostatic activity for wound healing, *Adv. Healthcare Mater.* 11 (12) (2022) 2102367, <https://doi.org/10.1002/adhm.202102367>.
- [46] H. Wang, X. Li, B. Luo, K. Wei, G. Zeng, The MXene/water nanofluids with high stability and photo-thermal conversion for direct absorption solar collectors: a comparative study, *Energy* 227 (2021) 120483, <https://doi.org/10.1016/j.energy.2021.120483>.
- [47] N. Aslfattahi, et al., Efficiency enhancement of a solar dish collector operating with a novel soybean oil-based-MXene nanofluid and different cavity receivers, *J. Clean. Prod.* 317 (2021) 128430, <https://doi.org/10.1016/j.jclepro.2021.128430>.
- [48] Z. Said, et al., Energy, exergy, economic and environmental (4E) analysis of a parabolic trough solar collector using MXene based silicone oil nanofluids, *Sol. Energy Mater. Sol. Cell.* 239 (2022) 111633, <https://doi.org/10.1016/j.solmat.2022.111633>.
- [49] M. Mao, et al., Ti₃C₂T_x MXene nanofluids with enhanced thermal conductivity, *Chemical Thermodynamics and Thermal Analysis* 8 (2022) 100077, <https://doi.org/10.1016/j.ctta.2022.100077>.
- [50] Z. Bao, N. Bing, X. Zhu, H. Xie, W. Yu, Ti₃C₂T_x MXene contained nanofluids with high thermal conductivity, super colloidal stability and low viscosity, *Chem. Eng. J.* 406 (2021) 126390, <https://doi.org/10.1016/j.cej.2020.126390>.
- [51] S.A. Abdollahi, et al., Combining artificial intelligence and computational fluid dynamics for optimal design of laterally perforated finned heat sinks, *Results in Engineering* (2024) 102002, <https://doi.org/10.1016/j.rineng.2024.102002>.
- [52] S.A. Abdollahi, et al., A novel insight into the design of perforated-finned heat sinks based on a hybrid procedure: computational fluid dynamics, machine learning, multi-objective optimization, and multi-criteria decision-making, *Int. Commun. Heat Mass Tran.* 155 (2024) 107535, <https://doi.org/10.1016/j.icheatmasstran.2024.107535>.
- [53] H. Fattahi, M. Hasanipannah, N. Zandy Ilghani, Investigating correlation of physico-mechanical parameters and P-wave velocity of rocks: a comparative intelligent study, *Journal of Mining and Environment* 12 (3) (2021) 863–875.
- [54] H. Fattahi, N. Zandy Ilghani, Hybrid wavelet transform with artificial neural network for forecasting of shear wave velocity from wireline log data: a case study, *Environ. Earth Sci.* 80 (1) (2021) 1–10, <https://doi.org/10.1007/s12665-020-09320-9>.
- [55] H. Fattahi, N. Zandy Ilghani, Application of Monte Carlo Markov chain and GMDH neural network for estimating the behavior of suction caissons in clay, *Geotech. Geol. Eng.* (2023) 1–15, <https://doi.org/10.1007/s10706-023-02455-z>.
- [56] M. Jamei, Z. Said, Recent advances in the prediction of thermophysical properties of nanofluids using artificial intelligence, *Hybrid Nanofluids* (2022) 203–232, <https://doi.org/10.1016/b978-0-323-85836-6.00009-0>.
- [57] Q. Nguyen, R. Rizvandi, A. Karimipour, O. Malekhamadi, Q.-V. Bach, A novel correlation to calculate thermal conductivity of aqueous hybrid graphene oxide/silicon dioxide nanofluid: synthesis, characterizations, preparation, and artificial neural network modeling, *Arabian J. Sci. Eng.* 45 (2020) 9747–9758, <https://doi.org/10.1007/s13369-020-04885-w>.
- [58] S. Rostami, A.A. Nadooshan, A. Raisi, M. Bayareh, Modeling the thermal conductivity ratio of an antifreeze-based hybrid nanofluid containing graphene oxide and copper oxide for using in thermal systems, *J. Mater. Res. Technol.* 11 (2021) 2294–2304, <https://doi.org/10.1016/j.jmrt.2021.02.044>.
- [59] M. Ibrahim, T. Saeed, A.M. Alshehri, Y.-M. Chu, Using artificial neural networks to predict the rheological behavior of non-Newtonian graphene-ethylene glycol nanofluid, *Journal of Thermal Analysis and Calorimetry* 145 (4) (2021) 1925–1934, <https://doi.org/10.1007/s10973-021-10682-w>.
- [60] N. Parashar, N. Aslfattahi, S.M. Yahya, R. Saidur, An artificial neural network approach for the prediction of dynamic viscosity of MXene-palm oil nanofluid using experimental data, *Journal of Thermal Analysis and Calorimetry* 144 (2021) 1175–1186, <https://doi.org/10.1007/s10973-020-09638-3>.
- [61] S. Tian, N.I. Arshad, D. Toghraie, S.A. Eftekhari, M. Hekmatifar, Using perceptron feed-forward Artificial Neural Network (ANN) for predicting the thermal

- conductivity of graphene oxide-Al₂O₃/water-ethylene glycol hybrid nanofluid, *Case Stud. Therm. Eng.* 26 (2021) 101055, <https://doi.org/10.1016/j.csite.2021.101055>.
- [62] N. Parashar, N. Aslfattahi, S.M. Yahya, R. Saidur, ANN modeling of thermal conductivity and viscosity of MXene-based aqueous ionanofluid, *Int. J. Thermophys.* 42 (2021) 1–24, <https://doi.org/10.1007/s10765-020-02779-5>.
- [63] N. Parashar, J. Khan, N. Aslfattahi, R. Saidur, S.M. Yahya, Prediction of the dynamic viscosity of MXene/palm oil nanofluid using support vector regression, in: *Recent Trends in Thermal Engineering: Select Proceedings of ICCEMME 2021*, Springer, 2022, pp. 49–55, https://doi.org/10.1007/978-981-16-3428-4_5.
- [64] N.B. Shaik, et al., Artificial neural network modeling and optimization of thermophysical behavior of MXene Ionanofluids for hybrid solar photovoltaic and thermal systems, *Therm. Sci. Eng. Prog.* 33 (2022) 101391, <https://doi.org/10.1016/j.tsep.2022.101391>.
- [65] Z. Said, et al., Synthesis, stability, density, viscosity of ethylene glycol-based ternary hybrid nanofluids: experimental investigations and model-prediction using modern machine learning techniques, *Powder Technol.* 400 (2022) 117190, <https://doi.org/10.1016/j.powtec.2022.117190>.
- [66] S. Alqaed, J. Mustafa, M. Sharifpur, G. Cheraghian, The effect of graphene nanopowder on the viscosity of water: an experimental study and artificial neural network modeling, *Nanotechnol. Rev.* 11 (1) (2022) 2768–2785, <https://doi.org/10.1515/ntrev-2022-0155>.
- [67] C. Boobalan, S.K. Kannaiyan, A correlation to predict the thermal conductivity of MXene-silicone oil based nano-fluids and data driven modeling using artificial neural networks, *Int. J. Energy Res.* 46 (15) (2022) 21538–21547, <https://doi.org/10.1002/er.7786>.
- [68] Z. Said, P. Sharma, N. Aslfattahi, M. Ghodbane, Experimental analysis of novel ionic liquid-MXene hybrid nanofluid's energy storage properties: model-prediction using modern ensemble machine learning methods, *J. Energy Storage* 52 (2022) 104858, <https://doi.org/10.1016/j.est.2022.104858>.
- [69] P.K. Kanti, P. Sharma, B. Koneru, P. Banerjee, K.D. Jayan, Thermophysical profile of graphene oxide and MXene hybrid nanofluids for sustainable energy applications: model prediction with a Bayesian optimized neural network with K-cross fold validation, *FlatChem* 39 (2023) 100501, <https://doi.org/10.1016/j.flatc.2023.100501>.
- [70] X. Ma, L. Yang, J. Song, W. Jiang, X. Li, X. Wu, Investigation on the stability, thermal conductivity and viscosity of MXene/water nanofluids and development of ANN models, *Powder Technol.* (2023) 118686, <https://doi.org/10.1016/j.powtec.2023.118686>.
- [71] N.K. Pvr, S. Venkatachalapathy, P. Kalidoss, P. Chaupal, Experimental investigation with ANN modeling of thermal conductivity and viscosity of a ternary nanofluid at different mixing ratios and volume concentrations, *J. Mol. Liq.* 383 (2023) 122006, <https://doi.org/10.1016/j.molliq.2023.122006>.
- [72] P.K. Kanti, P. Sharma, K. Sharma, M. Maiya, The effect of pH on stability and thermal performance of graphene oxide and copper oxide hybrid nanofluids for heat transfer applications: application of novel machine learning technique, *J. Energy Chem.* 82 (2023) 359–374, <https://doi.org/10.1016/j.jechem.2023.04.001>.
- [73] P.K. Kanti, P. Sharma, M.P. Maiya, K.V. Sharma, The stability and thermophysical properties of Al₂O₃-graphene oxide hybrid nanofluids for solar energy applications: application of robust autoregressive modern machine learning technique, *Sol. Energy Mater. Sol. Cell.* 253 (2023) 112207, <https://doi.org/10.1016/j.solmat.2023.112207>.
- [74] A. Ariyarat, et al., Predictive modeling of engine performance and emissions for castor oil ethyl ester biodiesel blends: a Gaussian process regression approach, *Results in Engineering* (2024) 102362, <https://doi.org/10.1016/j.rineng.2024.102362>.
- [75] J. Jayasinghe, P. Ekanayake, O. Panahatipola, C.I. Madhushani, U. Rathnayake, Forecasting the power generation at renewable power plants in Sri Lanka using regression trees, *Results in Engineering* 22 (2024) 102111, <https://doi.org/10.1016/j.rineng.2024.102111>.
- [76] M. Alsehli, et al., Insights into water-lubricated transport of heavy and extra-heavy oils: application of CFD, RSM, and metaheuristic optimized machine learning models, *Fuel* 374 (2024) 132431, <https://doi.org/10.1016/j.fuel.2024.132431>.
- [77] M. Jamei, et al., On the specific heat capacity estimation of metal oxide-based nanofluid for energy perspective—A comprehensive assessment of data analysis techniques, *Int. Commun. Heat Mass Tran.* 123 (2021) 105217, <https://doi.org/10.1016/j.jcheatmasstransfer.2021.105217>.
- [78] M. Gholizadeh, M. Jamei, I. Ahmadianfar, R. Pourrajab, Prediction of nanofluids viscosity using random forest (RF) approach, *Chemometr. Intell. Lab. Syst.* 201 (2020) 104010, <https://doi.org/10.1016/j.chemolab.2020.104010>.
- [79] A. Naseri, M. Jamei, I. Ahmadianfar, M. Behbahani, Nanofluids thermal conductivity prediction applying a novel hybrid data-driven model validated using Monte Carlo-based sensitivity analysis, *Eng. Comput.* (2020) 1–25, <https://doi.org/10.1007/s00366-020-01163-z>.
- [80] R. Pourrajab, I. Ahmadianfar, M. Jamei, M. Behbahani, A meticulous intelligent approach to predict thermal conductivity ratio of hybrid nanofluids for heat transfer applications, *Journal of Thermal Analysis and Calorimetry* 146 (2) (2021) 611–628, <https://doi.org/10.1007/s10973-020-10047-9>.
- [81] M. Jamei, I. Ahmadianfar, A rigorous model for prediction of viscosity of oil-based hybrid nanofluids, *Phys. Stat. Mech. Appl.* 556 (2020) 124827, <https://doi.org/10.1016/j.physa.2020.124827>.
- [82] M. Jamei, M. Karbasi, I.A. Olumegbon, M. Mosharaf-Dehkordi, I. Ahmadianfar, A. Asadi, Specific heat capacity of molten salt-based nanofluids in solar thermal applications: a paradigm of two modern ensemble machine learning methods, *J. Mol. Liq.* 335 (2021) 116434, <https://doi.org/10.1016/j.molliq.2021.116434>.
- [83] M. Jamei, I.A. Olumegbon, M. Karbasi, I. Ahmadianfar, A. Asadi, M. Mosharaf-Dehkordi, On the thermal conductivity assessment of oil-based hybrid nanofluids using extended kalman filter integrated with feed-forward neural network, *Int. J. Heat Mass Tran.* 172 (2021) 121159, <https://doi.org/10.1016/j.ijheatmasstransfer.2021.121159>.
- [84] Z. Zhang, et al., Optimized ANFIS models based on grid partitioning, subtractive clustering, and fuzzy C-means to precise prediction of thermophysical properties of hybrid nanofluids, *Chem. Eng. J.* (2023) 144362, <https://doi.org/10.1016/j.ccej.2023.144362>.
- [85] X. Zhang, et al., Mixed-decomposed convolutional network: a lightweight yet efficient convolutional neural network for ocular disease recognition, *CAAI Trans. Intell. Technol.* (2023) 1–14, <https://doi.org/10.1049/cit2.12246>.
- [86] Z. Li, S. Li, Recursive recurrent neural network: a novel model for manipulator control with different levels of physical constraints, *CAAI Trans. Intell. Technol.* 8 (3) (2023) 622–634, <https://doi.org/10.1049/cit2.12125>.
- [87] Z. Ding, et al., A structural developmental neural network with information saturation for continual unsupervised learning, *CAAI Trans. Intell. Technol.* 8 (3) (2023) 780–795, <https://doi.org/10.1049/cit2.12169>.
- [88] A. Koy, A.B. Çolak, The intraday high-frequency trading with different data ranges: A comparative study with artificial neural network and vector autoregressive models, *Arch. Ad. Eng. Sci.* (2023), <https://doi.org/10.47852/bonviewAAES32021325>.
- [89] W. Jin, et al., Investigation of thermal conductivity enhancement of water-based graphene and graphene/MXene nanofluids, *J. Mol. Liq.* 367 (2022) 120455, <https://doi.org/10.1016/j.molliq.2022.120455>.
- [90] F.J. Gravetter, L.B. Wallnau, L.-A.B. Forzano, J.E. Witnauer, *Essentials of Statistics for the Behavioral Sciences*, Cengage Learning, 2020.
- [91] A. Desgagné, P. Lafaye de Micheaux, A powerful and interpretable alternative to the Jarque-Bera test of normality based on 2nd-power skewness and kurtosis, using the Rao's score test on the APD family, *J. Appl. Stat.* 45 (13) (2018) 2307–2327, <https://doi.org/10.1080/02664763.2017.1415311>.
- [92] F. Andy, *Discovering statistics using SPSS 1* (2009).
- [93] P.K. Sen, Estimates of the regression coefficient based on Kendall's tau, *J. Am. Stat. Assoc.* (1968) 1379–1389, <https://doi.org/10.2307/2285891>.
- [94] K. Hornik, M. Stinchcombe, B. White, Multilayer feedforward networks are universal approximators, *Neural Network.* 2 (5) (1989) 359–366, [https://doi.org/10.1016/0893-6080\(89\)90020-8](https://doi.org/10.1016/0893-6080(89)90020-8).
- [95] K. Hornik, Approximation capabilities of multilayer feedforward networks, *Neural Network.* 4 (2) (1991) 251–257, [https://doi.org/10.1016/0893-6080\(91\)90009-t](https://doi.org/10.1016/0893-6080(91)90009-t).
- [96] S. Haykin, *Network, A comprehensive foundation*, *Neural Network.* 2 (2004) (2004) 41.
- [97] J. Wu, X.-Y. Chen, H. Zhang, L.-D. Xiong, H. Lei, S.-H. Deng, Hyperparameter optimization for machine learning models based on Bayesian optimization, *Journal of Electronic Science and Technology* 17 (1) (2019) 26–40.
- [98] A.H. Victoria, G. Maragatham, Automatic tuning of hyperparameters using Bayesian optimization, *Evolving Systems* 12 (2021) 217–223, <https://doi.org/10.1007/s12530-020-09345-2>.
- [99] R.J.J. Molu, et al., Advancing short-term solar irradiance forecasting accuracy through a hybrid deep learning approach with bayesian optimization, *Results in Engineering* (2024) 102461, <https://doi.org/10.1016/j.rineng.2024.102461>.
- [100] J. Wilson, F. Hutter, M. Deisenroth, Maximizing acquisition functions for Bayesian optimization, *Adv. Neural Inf. Process. Syst.* 31 (2018).
- [101] W. Gan, Z. Ji, Y. Liang, Acquisition functions in bayesian optimization, in: *2021 2nd International Conference on Big Data & Artificial Intelligence & Software Engineering (ICBASE)*, IEEE, 2021, pp. 129–135, <https://doi.org/10.1109/icbase53849.2021.00032>.
- [102] C.J. Willmott, Some comments on the evaluation of model performance, *Bull. Am. Meteorol. Soc.* 63 (11) (1982) 1309–1313, [https://doi.org/10.1175/1520-0477\(1982\)063<1309:scoteo>2.0.co;2](https://doi.org/10.1175/1520-0477(1982)063<1309:scoteo>2.0.co;2).
- [103] H. Pham, A new criterion for model selection, *Mathematics* 7 (12) (2019) 1215, <https://doi.org/10.3390/math7121215>.
- [104] H. Maleki, M. Ashrafi, N.Z. Ilghani, M. Goodarzi, T. Muhammad, Pareto optimal design of a finned latent heat thermal energy storage unit using a novel hybrid technique, *J. Energy Storage* 44 (2021) 103310, <https://doi.org/10.1016/j.est.2021.103310>.